

Sandpiles — Self Organized Critical Systems

Daniel Schmeier and Oliver Freyermuth

Winter Term 2010/2011

Abstract

In this essay we will describe the basic properties of the BAK-TANG-WIESENFELD model of sandpiles and analyze the structure of avalanches in the critical state for different configurations and dimensions of the system. We will show that avalanche properties fulfill power law behaviours, whose critical exponents we will determine, and scaling relations which we will derive and prove numerically. We will further analyse the dissipation of the system and show theoretically and with the simulated data that the frequency spectrum has a $1/f^\alpha$ form as can also be seen in many other physical topics. A separate analysis of the flow over the rim and inside the system will be performed and qualitatively checked against experimental results.

1 Introduction

The basic principles of how sandpiles evolve are something one is usually confronted with as a child at a sunny day on the beach: Sand is randomly distributed in space and time on a finite area and slowly the single grains form a pile, whose slope becomes steeper and steeper, until it reaches some maximum. If the pile has reached this state, any additional grain of sand will tumble down on the side to the floor. But even more than that: It can happen that it takes other grains with it such that an avalanche occurs, which may have arbitrary size up to the whole area of the pile. To grasp this behaviour in a more theoretical approach, one may say the system evolves to a critical state, where interactions over all length- and timescales can occur by simple natural evolution: This property can be found in many systems, for example in the development of earthquakes or forest fires, and was classified by BAK, TANG and WIESENFELD as *self-organised criticality* [BTW87]. The following sections will analyse this behaviour by using the BAK-TANG-WIESENFELD model for sandpiles. In section 2 we will explain the properties of this model and how a critical state

can be reached. In section 3 we will provide a deeper analysis of the structure of the critical state: We will formulate definitions of different observables and motivate that they are subject to scaling relations in the critical state which we will verify by measuring scaling exponents numerically and test for the relations to be fulfilled.. Furthermore, we will give a short overview on $1/f^\alpha$ -noise in physics and discuss its occurrence in our model in section 4, also providing a separate analysis of the flow in the interior and over the rim. The theoretical expectations will be checked against the simulated dissipation in the automaton and experimental results. In the final section 5 we will sum up the results of our measurements and give some outreach to other interesting measurements and theoretical considerations in the context of sandpiles and self-organised criticality.

2 Definitions and Setups

2.1 Sandpile Automata

A cellular automaton is a system consisting of a d -dimensional grid of *cells* which contain discrete values. These cells have a well-defined

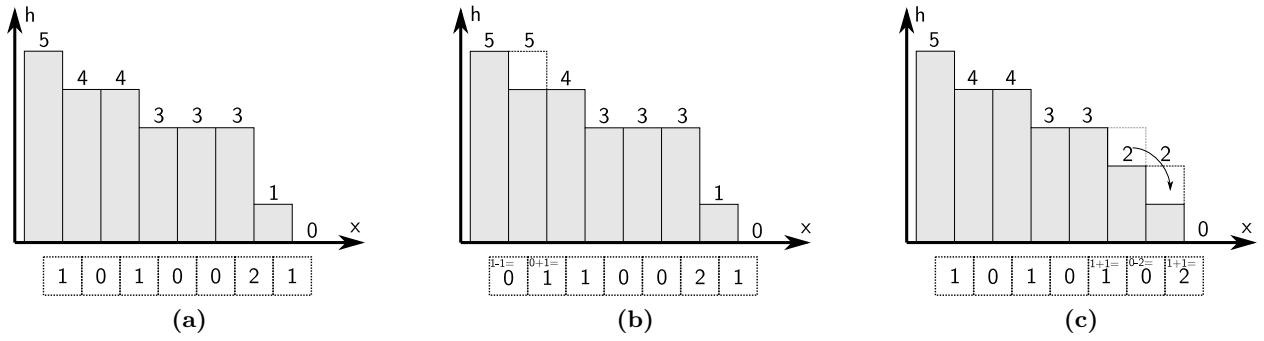


Figure 1. Visualisation of the 1-dimensional sandpile automata rules. a) A cell contains the discrete slope value $s_i = h_i - h_{i+1}$, where the heights are just imaginary bookkeeping objects for motivating the rules; they are never calculated actually. b) Adding a grain of sand at a point increases the slope value at one cell and decreases it at a neighbouring cell. c) If the slope at a point surpasses a critical value (here: 1), sand will tumble down by itself which means that the slope decreases by two units at a cell and is increased by one unit at the neighbouring cells.

neighbourhood relation and their values are updated in discrete time steps.

Definition We begin the explanation of our automata with the 1-dimensional case, since its rules can be understood intuitively: Let's assume we have a chain of points and each of those points has an assigned value of the pile height at that point. The height values can only have integer values and each unit represents one grain of sand. Then we define the cells $s_0 \dots s_{N-1}$ of our automaton as the space between two points and assign it the discretised slope at that point: $s_i := h_i - h_{i+1}$. We will always work in the slope picture and only use the heights as auxiliary quantities. Fig. 1a visualizes this definition.

Perturbation The system somehow needs to be driven from the ground state to the critical state by some mechanism of perturbation. Perturbation in the sandpile picture means adding sand. In our above definition of the 1 dimensional sandpile, adding a grain of sand at a random spot means that the slope at a random position is increased by one unit and the slope at the left neighbour cell is decreased by one unit, as one can easily verify using fig. 1b. This mechanism is called *conservative* perturbation, since it conserves the total amount of slope. For the simulation of the behaviour of the critical system it is also convenient to define a mechanism which increases the total slope and therefore performs a faster criticalisation of the system. This

mechanism is called *nonconservative perturbation* and just increases the slope at a random cell by 1 unit.

Relaxation The reason we work in the slope picture is because this is the observable which leads to the criticality of the system: If the slope overcomes a constant critical value s_{crit} , grains will tumble down and by itself drive the slope back to a noncritical value. Fig. 1c shows this for $s_{\text{crit}} = 1$: If one cell reaches a value of 2, it will decrease by 2 and the neighbouring cells will increase their values by 1. If one or even both neighbouring cells had the maximum slope value, the relaxation can lead to further relaxations, until all slopes reach a noncritical value. This is the *avalanche effect* and is very important for later considerations.

Boundaries Since we cannot simulate an infinite area on a computer, we have boundaries at s_0 and s_{N-1} and need to specify the behaviour of the system there. There are two commonly used types of boundaries: *Open* boundaries connect the most right point containing height information to the ground with constant height 0. This means that if the most right cell s_{N-1} relaxes, its slope only decreases by 1 value. Alternatively, the boundary can be *closed*. This means, that sand at the boundary cannot tumble and therefore the rightmost cell has a constant slope value of 0.

When defining the boundary conditions, we only considered the rightmost boundary. The

leftmost boundary is always considered to be closed, since we assume that the sandpiles are symmetric. We only deal with piles which evolve in a mountain-like structure as in fig. 1a, so the height decreases from left to right. We now subsume the rules described above:

| | |
|-------------------------------|---|
| General relaxation: | |
| $s_n > s_{\text{crit}}$ | $s_n \rightarrow s_n - 2$ $s_{n\pm 1} \rightarrow s_{n\pm 1} + 1$ |
| Closed border: | |
| | $s_0 = 0$ |
| Open border: | |
| $s_{N-1} > s_{\text{crit}}$ | $s_{N-1} \rightarrow s_{N-1} - 1$ $s_{N-2} \rightarrow s_{N-2} + 1$ |
| Conservative Perturbation: | |
| | $s_n \rightarrow s_n + 1$ $s_{n-1} \rightarrow s_{n-1} - 1$ |
| Nonconservative Perturbation: | |
| | $s_n \rightarrow s_n + 1$ |

2 Dimensions In more than one dimension, the rules for the dynamics of the slopes stay exactly the same and can thus be generalised easily. However, the evolution of a system with more than 1 dimension will be completely different, which can be easily realised by going back to the basic principle introduced in section 1: A two dimensional pile, for example found in an hourglass, shows a special behaviour in the way that avalanches may interact or trigger avalanches of different size at another position on the lattice. A similar behaviour may be observed when using slightly wet sand on the beach and building a very steep pile of sand. As soon as the water evaporates, avalanches evolve and the slope of the pile begins to shrink. This very much corresponds to the random perturbation we are applying to our simulated system.

Starting with two dimensions, we may think again about the correspondence between slopes and heights: The relation is now more complex, a direct correspondence between height and slope is not possible anymore. We define an *average local slope* s_{ij} using neighbouring bonds to a point in the slope-lattice as illustrated in fig. 2 by using the relation: $s_{ij} = h_1 + h_2 - h_3 - h_4$.

For the stabilisation process, this corresponds to two grains of sand tumbling from the bonds 1 and 2 to 3 and 4, thus reducing the average local slope (which we will from now on call slope again) by 4.

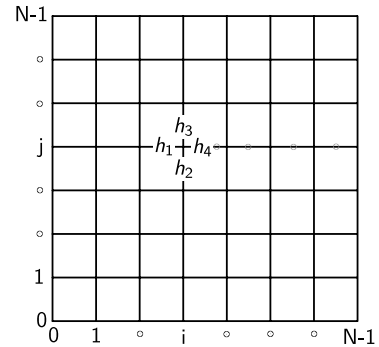


Figure 2. Parametrisation of the slope based on the height of piles in 2 dimensions. Illustration based on [CFJJ91]

Applying perturbation, a conservative perturbation corresponds to the addition of a grain of sand to each of the lower-left bonds 1 and 2, thus increasing the slope by 2. The nonconservative perturbation is more complex, for we defined it having the slope picture in mind: Adding one to the slope locally means removing 1 grain of sand on each bond in direction 3 or 4 (as marked with grey dots in direction 4 in fig. 2) or instead adding one grain to each bond in direction 1 or 2. This does not directly correspond to the physical picture one has in mind, but indeed leads to faster criticalisation in the slope picture. Concerning the heights, a distribution like that provided in fig. 3 evolves.

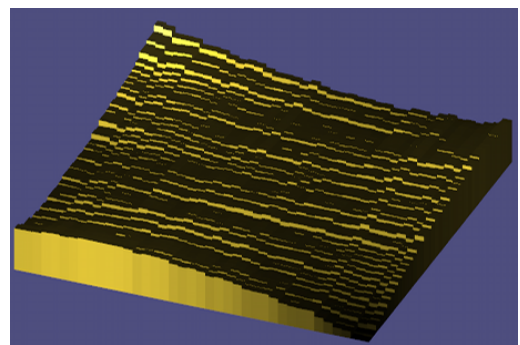


Figure 3. Evolution of the height in a closed 2 dimensional lattice which is subject to nonconservative perturbation

One may notice that the description in the classic height model becomes even more com-

plex in higher dimensions (especially keeping the simulation itself in mind). For that reason, in higher dimensions we will limit ourselves to the slope model only.

d Dimensions In more than 2 dimensions, the rules essentially stay the same. Using the relations already described in section 2.1, we can simply derive the general rules for all dimensions by replacing the change in slope by a value dependent on the dimension of the system. Taking the stabilisation step, now not only two grains of sand tumble as was the case in 2 dimensions, but d grains change place. For that reason, the slope is reduced by an amount of $2 \cdot d$. The definitions of the perturbations are generalised in a very similar way: Now, all axes are taken into account, thus the conservative perturbation increases the local slope by d and reduces the slope by 1 in each neighbouring site closer to the lower border of the lattice.

The major change one has to keep in mind is that the amount of border-areas grows fast with each dimension. For that reason, boundary effects play a much higher role the higher the dimension of the system is.

Further details on the measured observables and the general behaviour will be discussed in section 3. The generalisation of the rules for the multidimensional case can be subsumed as follows, while we always define the lower borders as closed (for symmetry reasons) and the upper borders at $N - 1$ as closed or open depending on the analysed system:

General relaxation:

$$s_{\vec{n}} > s_{\text{crit}} : \\ s_{\vec{n}} \rightarrow s_{\vec{n}} - 2 \cdot d \quad (1)$$

$$s_{\vec{n} \pm \vec{e}_i} \rightarrow s_{\vec{n} \pm \vec{e}_i} + 1 \quad i = 1, \dots, d$$

Closed border:

$$s_{\vec{n}} = 0 \quad \exists \vec{n}_i = 0 \quad i = 1, \dots, d$$

Open border:

$$s_{\vec{n}} > s_{\text{crit}} : \\ s_{\vec{n}} \rightarrow s_{\vec{n}} - 2 \cdot d + \text{count}(i | \vec{n}_i = N - 1)$$

$$s_{\vec{n} + \vec{e}_i} \rightarrow s_{\vec{n} + \vec{e}_i} + 1 \quad |\vec{n}_i \neq N - 1 \\ s_{\vec{n} - \vec{e}_i} \rightarrow s_{\vec{n} - \vec{e}_i} + 1 \quad i = 1, \dots, d \quad (2)$$

Conservative Perturbation:

$$s_{\vec{n}} \rightarrow s_{\vec{n}} + d \\ s_{\vec{n} - \vec{e}_i} \rightarrow s_{\vec{n} - \vec{e}_i} - 1 \quad i = 1, \dots, d$$

Nonconservative Perturbation:

$$s_{\vec{n}} \rightarrow s_{\vec{n}} + 1$$

2.2 Evolution of the System

After implementing the rules given in section 2, we can observe the dynamics of the system in different dimensions, for different perturbation mechanisms and with different boundary conditions. In this section, we will analyse how the system evolves if we start from scratch (all cells set to 0) and if/how criticality is reached.

For describing the state of the system, we will make use of the *average slope*, defined as the arithmetic mean of all cell entries:

$$\langle s \rangle (t) = \frac{1}{N^d} \cdot \sum_{\vec{n}} s_{\vec{n}}(t) \quad (3)$$

Since the slope is the transmitted information of the system, it seems intuitive to check how this value changes during the evolution of the system and how the differences in boundaries or perturbations can be seen here. In example figures, we measured the time evolution only for one run, since we do not want a statistically clean measure of the evolution but an image of how a specific system behaves. They are done on a two dimensional 40×40 grid to keep comparability with [CFJJ91] and a critical slope of 7, which is also used for all other data in this thesis in all dimensions.¹

Closed Boundaries The easier but at the same time special case is the closed boundary system. In the slope-model, the outer boundary cells are constantly set to 0 and thus no sand can leave the system (a slope of 0 means an equality of the height of the piles). We first have a look at the effect of conservative perturbation: Close to the lower boundaries, the constantness

¹One should note that the behaviour of the system does not really depend on the actual value of s_{crit} : A higher value just lengthens the time from startup to the critical state

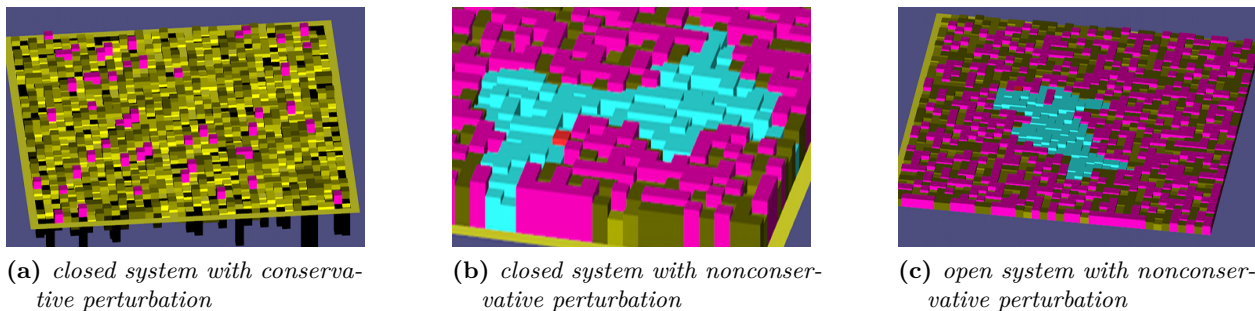


Figure 4. The red site marks the origin of the perturbation, the blue sites are all sites affected by the single avalanche. The pink sites are all critical sites, i.e. an avalanche can be triggered by performing a perturbation at these sites.

of closed boundaries “swallows” the subtracting step, whereas on the upper boundaries at $N - 1$, the adding–slope–steps of the perturbations are absorbed. So every perturbation on the interior keeps the slope constant, whereas the swallowing effects on the boundaries cancel each other, so globally the average slope can not rise and get critical! It even decreases over time, since relaxation on close boundaries can lead to loss of total slope, which is exactly what can be observed in fig. 4a: Only few sites are critical, avalanches are small and negative slope can be observed at many sites. This effect can be observed in all the dimensions we analysed and only the speed of the evolution depends on the lattice size. The heights of the sandpiles on all sites evolve in a very natural way: They simply grow continuously with equally distributed heights. In fig. 5b, we also see how the average slope drops continuously for closed boundary conditions and that we never end up in a critical state. We will therefore omit this case from now on, since we are only interested in critical phenomena which this configuration clearly does not possess.

Using nonconservative perturbation, we only increase the local slope by 1. This leads to a more interesting behaviour: The slopes can now only decrease by the stabilisation process, and any surplus on slope is absorbed at the boundaries. This system reaches a state of criticality, in which every further perturbation has a high probability of triggering a local or a global avalanche over the whole size of the lattice. Looking at $\langle s \rangle$, we see that the critical state the system ends up in does not really change its average slope anymore (despite some small

fluctuations), even if we perturbate further and further. So relaxation and perturbation lead to by itself into a critical state, a so called ATTRACTOR which is not lost anymore once reached. BAK, TANG and WIESENFELD called this principle “Self-Organized Criticality” and it can be found in many other systems driven by local rules, e.g. the evolution of fire forests or earthquakes. The fact that the criticality is never lost, even if we perturbate further and further, is an important feature and has to be emphasized at this point, since this is necessary to do any statistical relevant measurements later on on this set of critical states.

Looking at $\langle s \rangle$, we see that the asymptotic value lies under the critical slope. This is because from 1600 points we have 156 boundary points with constant 0 slope in the case of closed boundary conditions. But even if all other non–boundary–points would be at their critical value, the average slope would be 6.31, but we see 5.46. This is an interesting fact, which is true for all dimensions higher than 1²: The asymptotic case where the system drives itself into is *not* the one where all cells contains the critical value, but it is an ensemble of different configurations: Several cells lie below the critical value here, which basically is caused by the relaxation process: If a cell is critical, it stays critical, but once it comes over the critical value, it decreases itself by $2d$, which ends up *below* the critical value. So in the end, we assume a stable critical configuration containing cells with values within $s_{\text{crit}} - 2d + 1$ and s_{crit} which is in agreement with

²In 1 dimension the system indeed will end up in a state with all cells critical and will always stay there. Therefore sometimes this case needs special treatment

our measured value. Since this interval depends on the dimensionality of the system, we checked the behaviour for different dimensions as well, which can be seen in fig. 5c: The higher the dimension, the longer it takes to reach the critical state, which is clear because the total amount of cells is larger so it needs more perturbation steps. But one also sees that the asymptotic value of the average slope decreases drastically for higher dimensions, which can be understood with the argumentation from before.

Open Boundaries Considering open boundaries in our model, the rules change for the upper boundaries (at $N - 1$ in each dimension): They are now treated like normal lattice sites, with the difference that in the stabilisation step the slopes can only distribute to neighbours that are available, i.e. only to 1 neighbour in the 1 dimensional model on the open border. The remaining slope is not lost, but remains at the lattice site. This corresponds to a reduction of the height of the pile at the lattice site when considering the rules for the 2 dimensional system (refer to section 2.1). When observing the behaviour of the system, this means that no slopes are absorbed at these boundaries, but rather conserved or even reflected back. In general, the system qualitatively behaves nearly similar to the closed-boundary-system with nonconservative perturbation, as can be seen in fig. 5a, the asymptotic value of 5.80 is slightly higher, since we have less zero counting closed cells. An image of the slope distribution in 2 dimensions can be observed in fig. 4c and also shows major similarity to the closed boundary case.

Using conservative perturbation, a new effect may be observed: In the closed case, the average slope was shrinking due to the absorption of slope in the boundary. In the open system, the system *collects* slope at the open boundary, for slope is never lost in the stabilisation step at this border. After many steps of continuous perturbation and stabilisation, a critical system can evolve which qualitatively also behaves mostly similar to the system produced by using nonconservative perturbation. Looking at the evolution of the average slope in 5b, we see that it takes a higher amount of time steps for the system to come to the critical case as in

the nonconservative case, since increasing the total slope can only happen by perturbing at the closed boundaries, as explained before. The asymptotic value is approximately the same, though.

Let's sum up the results of our comparison: The closed conservative case does not show any asymptotics and is therefore neglected from now. All other cases show a critical state after perturbing the system long enough: These critical states are ensembles of different configurations which fluctuate around the same average slope value. Further perturbation may change the configuration, but it will stay in the critical ensemble (it is, in this sense, ergodic). Systems, which show this behaviour, are named to possess self-organized criticality. For nonconservative open and nonconservative closed, only the average slope asymptotics change, the dynamics are quite similar. Conservative open systems need a much longer time to reach the critical state, but then they have reached the same average slope value as the nonconservative ones.

Reaching the critical state We have seen how the system drives itself into the critical state if we start from scratch and continuously perturbate the system if it is stable until criticality is reached. There is a different method of driving the system into criticality, which we call *overcriticalising*: We set each cell to a random value between $s_{\text{crit}} + 1$ and $2s_{\text{crit}}$, and let the system, which obviously is unstable then, relax via (1). The system will end up in the same critical ensemble, as one can see in fig. 6). Since relaxation happens simultaneously on all lattice cells it works much faster, not only on the level of time steps but also on processing time basis. This is why we will use this method of driving the system critical for the rest of this thesis.

3 Scaling Exponents

3.1 Avalanche Properties at Criticality

Definitions After the system has reached its critical state, for each perturbation it is very likely that an avalanche occurs which can change the system on small or large ranges. We are interested in how these avalanches behave and whether they underlie scaling relations as one

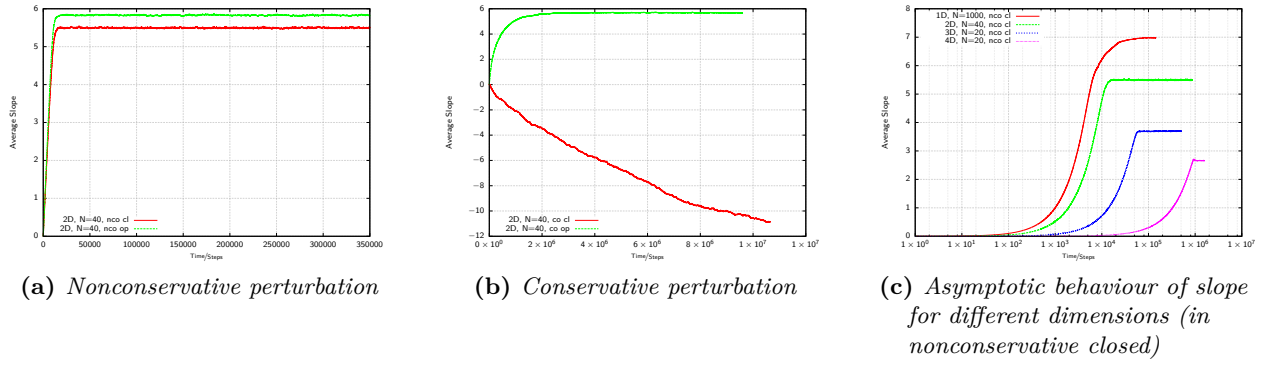


Figure 5. Time evolution of the average slope for different perturbation mechanisms, boundary conditions and dimensions

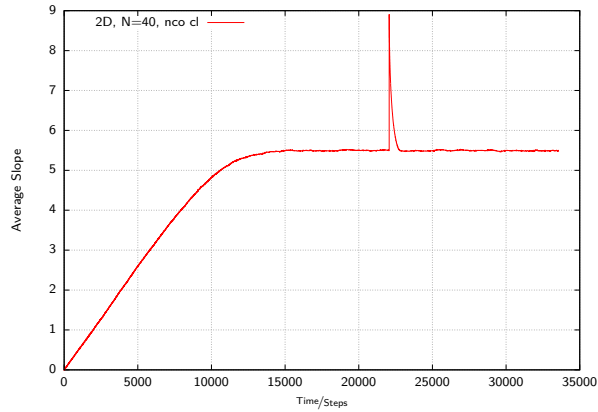


Figure 6. Comparison of criticalisation by starting from scratch and by overcriticalising the system

would expect from a critical system. To accomplish this task, we defined the following observables. First we define the *instantaneous dissipation rate* $f_\alpha(t)$ of an avalanche α :

$$f_\alpha(t) := \sum_{\vec{n}} \Theta(s_{\vec{n}}(t) > s_{\text{crit}}) \quad (4)$$

So it returns the amount of cells at a specific time step t which are going to relax in the next update of the lattice. It is called dissipation, since in the sandpile picture the sliding of sand to a lower level equals a loss of potential energy, so each slide lowers the total energy of the system. We define the *size of an avalanche* as the total amount of dissipation it creates:

$$s := \int_0^\infty f_\alpha(t) dt \quad (5)$$

The *lifetime* of an avalanche is the total amount of time steps where dissipation occurs:

$$t := \max(t|f_\alpha(t) > 0) - \min(t|f_\alpha(t) > 0) \quad (6)$$

Additionally we define the *radius* as the longest of all distances (which is the length of the shortest path over the lattice) from the starting point \vec{n}_0 of relaxation to any point the avalanche reaches

$$r := \max(d|d = |\vec{n}, \vec{n}_0|, \forall_{\vec{n}} \exists \tau : s_{\vec{n}}(\tau) > s_{\text{crit}}) \quad (7)$$

We analyzed the probability distributions of these observables in the critical state of the system under the assumption that they scale according to the behaviour of a critical system. Furthermore, we assume that these three stochastic variables in the critical case have certain relationships, from which we define the following *scaling exponents*:

$$\begin{aligned} P(S = s) &\approx s^{1-\tau} \\ P(T = t) &\approx t^{1-\alpha} \\ P(R = r) &\approx r^{1-\lambda} \\ E(S|T = t) &\approx t^{\gamma_1} \\ E(T|S = s) &\approx s^{1/\gamma_1} \\ E(S|R = r) &\approx r^{\gamma_2} \\ E(R|S = s) &\approx s^{1/\gamma_2} \\ E(T|R = r) &\approx r^{\gamma_3} \\ E(R|T = t) &\approx t^{1/\gamma_3} \end{aligned} \quad (8)$$

These assumptions are based on the fundamental properties of a critical system: It does not contain any intrinsic time and length scale, which

in the sandpile picture means that avalanches can both act locally on a small set of cells and globally over the whole size of the lattice. That this is the case comes from the fact that in the asymptotic state not all cells are critical: If this would be the case, than every avalanche would reach over the whole lattice. But since critical cells can happen to appear isolated, also small avalanches can occur. We see that $E(X|Y)$ and $E(Y|X)$ are defined using the same γ_i : If we assume that observable X and Y are related with a certain exponent, we also have to assume that conversely they are also related with the inverse exponent. This is something we are going to check by our data, where we will calculate γ_i and $1/\gamma_i$ independantly from each other.

We already stated, that the 1 dimensional case is special, since it is attracted to the state where all cells are critical. This is obviously not compatible with the above explanation for which in this section, the one dimensional case will not be treated.

Scaling Relations We have now defined many exponents which can basically be obtained by simulating experiments and fitting the exponential functions independently to the different distributions one gets. However, it turns out that if one treats the above definitions in a more theoretical sense then they are not independent at all, as we are now going to show (this proof is based on the one in [CFJJ91]):

Having three statistical observables X , Y and Z , we can relate them to each other by taking the following identity for $E(X)$:

$$\begin{aligned} & \int xP(X = x) dx \\ &= \int xP(X = x) \int P(Y = y) dx dy \quad (9) \\ &= \iint xP(X = x, Y = y) dx dy \\ &= \iint x \frac{P(X = x, Y = y)}{P(Y = y)} P(Y = y) dx dy \\ &= \iint xP(X = y|Y = y)P(Y = y) dx dy \\ &= \int E(X|Y = y)P(Y = y) dy \quad (10) \end{aligned}$$

Where from (9) on we could also have put Z instead of Y and then would receive a different version of (10). These two can be set equal

since they are both evolved from $E(X)$. Putting $X = S$, $Y = T$ and $Z = R$ we then get

$$\int t^{\gamma_1} t^{1-\alpha} dt = \int l^{\gamma_2} t^{1-\lambda} dl \quad (11)$$

Now we can transform t into l using our relation properties in (8): $L = T^{1/\gamma_3}$ and formulate the equality of the exponents on both sites. If we do so and do the same for other combinations (like $X = T, Y = S, Z = L$ etc.), we gain three independent relations which we can substitute into each other to simplify the results. One then gets the following set of scaling relations:

$$\begin{aligned} \gamma_2 &= \gamma_1 \cdot \gamma_3 \\ \alpha &= 2 + \frac{\lambda - 2}{\gamma_3} \\ \tau &= 2 + \frac{\lambda - 2}{\gamma_2} \end{aligned} \quad (12)$$

These relations will help us to check our data for consistency: We will fit the exponential behaviours in (8) independently from each other and then look whether the results although gained independently are in numerical agreement with each other concerning (12).

3.2 Simulation Results

Procedure To take measurement data, we use white-noise perturbation (adding slope at random positions and at random points in time) to generate a high amount of avalanches in different systems. Algorithmically, we always peturb random points one after another until an avalanche is created: We then start the measurement until the system is stabilized again, and then repeat the perturbation process. Another method would be to overcriticalise the system after each analysis by setting the individual lattice sites to random values well above s_{crit} , however, an analysis of the autocorrelation using this approach and the (by far faster) method of a *single perturbation* until an avalanche is triggered proofed that both methods are usable, so we took the latter. This also conforms to the idea of *self-organised criticality*, because the system criticalises itself after each avalanche because of ergodicity.

Determinating Scaling Exponents For measuring the exponents in (8), we first determined

all probability densities $P(X = x)$ and joint probability densities $P(X = x, Y = y)$ using the data we collected by producing a high amount of avalanches and measuring their properties. The latter are needed to calculate the conditional expectation values via:

$$\begin{aligned} E(X|X = y) &= \sum_x x \cdot P(X = x|Y = y) \\ &= \sum_x x \cdot \frac{P(X = x, Y = y)}{P(Y = y)} \quad (13) \end{aligned}$$

We draw the distributions in a double logarithmic representation, since here a power law scaling is represented by a straight line and therefore can be identified easily visually. One can see, that all distributions and expectation values indeed fulfill scaling relations, at least over one or more intermediate decades. Deviations from the assumed scaling behaviour were to be expected: Our simulations are affected by the discreteness of the lattice in the lower regions and by its finite size on the upper regions. We will take a closer look at the latter ones in the next paragraph.

To the intermediate scaling regions we performed a LEVENBERG–MARQUARD–Fit via the free tool GNUPLLOT [WKm08] to determine the critical exponents. The uncertainties on these exponents mostly evolve from manually choosing the ranges of the scaling area for fitting: These are sometimes difficult to identify because statistical fluctuations and/or overall curvatures make it difficult to identify the clear start and end of the intermediate region. We estimate an uncertainty on the exponents $\tau, \alpha, \lambda, \gamma_i$ of 0.05 for dimensions 2 and 3 and 0.1 für dimensions 4 and 5. The $1/\gamma_i$ have errors of 0.03 in 2 and 3 dimensions, 0.05 in 4 and 5 dimensions. The results for the exponents can be seen in tab. 1 and they show a very good agreement to results in [CFJJ91].

The values for the exponents and fig. 7 and 8 shows that the exponents depend on the dimension of the system. If this problem has a critical dimension from which on scaling exponents remain constant, it is larger than 4 according to these data, which is in agreement to results in [CFJJ91]. We tried to take data for the 6 dimensional case also, but statistics were not good enough to perform an analysis of comparable accuracy, but it seemed at first sight as if also

there a difference of the power law was visible so that probably the critical dimension is even higher than 5.

In tab. 2 we opposed values which according to the scaling relations in (12) should correspond to each other. We see only small discrepancies which lie within numerical accuracy. This numerically proves our statement, that the stationary system is critical and leads to fundamental scaling properties for the avalanches.

Finite Size Scaling As already explained, the asymptotic behaviour of the distribution functions can be explained by the discreteness of the lattice and its boundaries. We have taken a closer look at the finite size behaviour and checked whether deviations at higher regions really can be related to the boundaries of the lattice. We do this exemplarily for the radius of the avalanches at closed boundary conditions, since they make the system symmetric, and for the nonconservative perturbation mechanism. For this task we suggest a finite size scaling hypothesis: All effects caused by the size N of the lattice for the distribution of the scaling variable R depend on the ratio³ $(N-2)^\sigma/r$, with σ being, according to [BTW88], a dynamical critical exponent which has to be found. We make the following new scaling ansatz:

$$P(R = r) = r^{1-\lambda} \cdot F((N-2)^\sigma/r) \quad (14)$$

$$\text{with } F(x) \xrightarrow{x \rightarrow \infty} 1 \quad (15)$$

With this ansatz, we include the assumed finite size effect but also make sure that it vanishes if the orders of lattice size and radius differ to much and no effect should be visible. With reordering we get $P(R = r) \cdot r^{\lambda-1} = F((N-2)^\sigma/r)$, so by taking data we get $P(R = r)$ for different N , we determine the exponent λ for the midrange area and then draw $P(R = r) \cdot r^{\lambda-1}$ against $(N-2)^\sigma/r$ and check whether a σ exists such that all data for different N follows the same functional behaviour F . Fortunately, it does so for $\sigma \approx 1.00$, as can be seen in fig. 9. This value for σ is reasonable: The maximum radius for a given size N in two dimensions

³We have to take $N - 2$ instead of the commonly used N since we have to take into account that N includes two closed boundary cells which never contribute to avalanches.

| | | τ | α | λ | γ_1 | $1/\gamma_1$ | γ_2 | $1/\gamma_2$ | γ_3 | $1/\gamma_3$ |
|--------|-------|--------|----------|-----------|------------|--------------|------------|--------------|------------|--------------|
| co op | 2D 40 | 2.15 | 2.17 | 2.06 | 1.60 | 0.63 | 2.05 | 0.50 | 1.31 | 0.79 |
| | 3D 20 | 2.40 | 2.66 | 2.72 | 1.72 | 0.57 | 2.60 | 0.39 | 1.51 | 0.62 |
| | 4D 20 | 2.5 | 2.7 | 2.8 | 1.8 | 0.57 | 2.8 | 0.34 | 1.7 | 0.59 |
| | 5D 15 | 2.6 | 3.0 | 3.0 | 1.8 | 0.53 | 2.9 | 0.33 | 1.7 | 0.50 |
| nco op | 2D 40 | 2.05 | 2.05 | 1.96 | 1.56 | 0.64 | 2.05 | 0.49 | 1.33 | 0.77 |
| | 3D 20 | 2.31 | 2.49 | 2.51 | 1.74 | 0.56 | 2.78 | 0.38 | 1.69 | 0.61 |
| | 4D 20 | 2.3 | 2.7 | 3.6 | 1.7 | 0.56 | 2.9 | 0.31 | 1.7 | 0.58 |
| | 5D 15 | 2.5 | 2.9 | 3.7 | 1.7 | 0.51 | 3.3 | 0.34 | 1.9 | 0.54 |
| nco cl | 2D 40 | 2.03 | 2.07 | 2.03 | 1.58 | 0.61 | 1.98 | 0.50 | 1.28 | 0.78 |
| | 3D 20 | 2.36 | 2.72 | 3.26 | 1.72 | 0.55 | 2.52 | 0.38 | 1.42 | 0.64 |
| | 4D 20 | 2.6 | 2.8 | 3.5 | 1.8 | 0.53 | 3.2 | 0.31 | 1.9 | 0.61 |
| | 5D 15 | 2.6 | 3.2 | 3.7 | 2.0 | 0.50 | 3.7 | 0.29 | 2.1 | 0.50 |

Table 1. Scaling exponents determined by fitting to simulated probability distributions and conditional expectation values

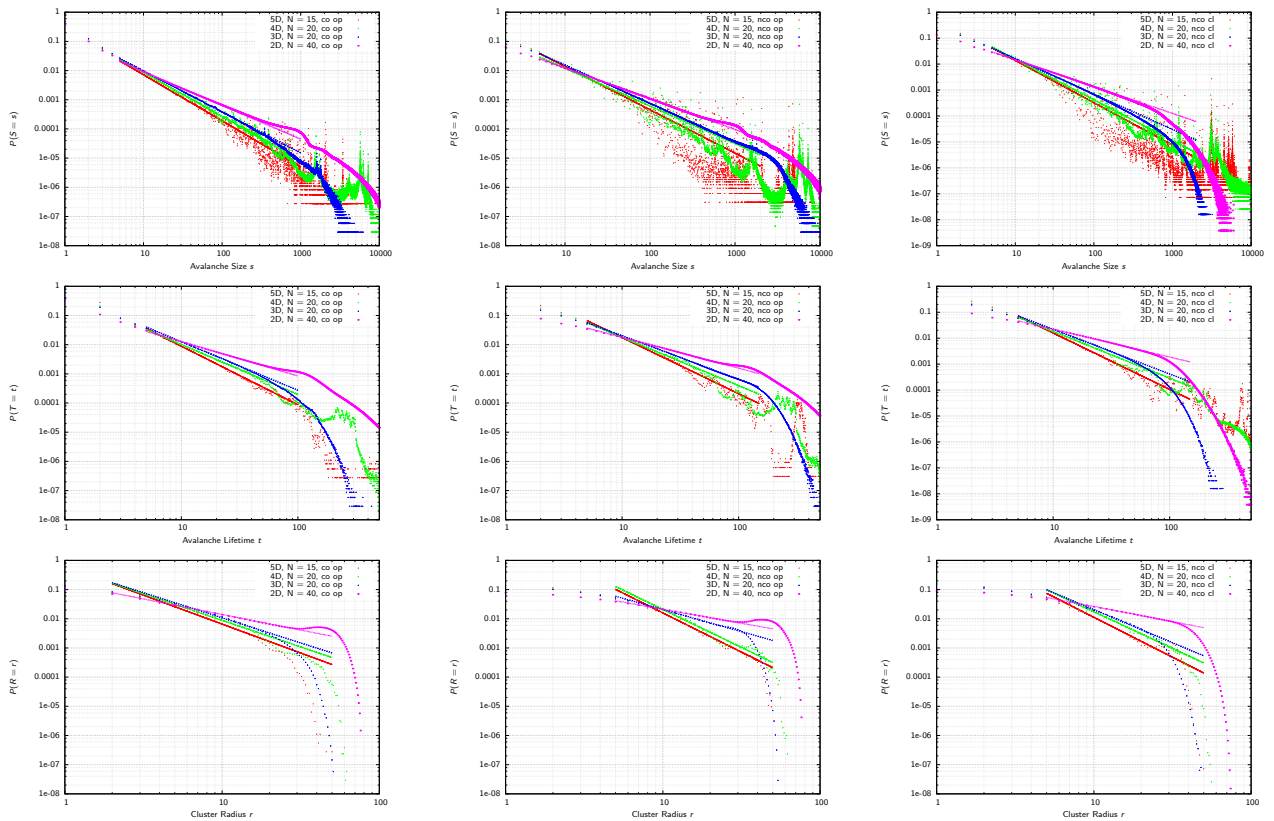


Figure 7. Probability distributions gained by simulating a high amount of independant avalanches and measuring their properties. Dots give the measured data, dashed lines the fitted power laws.

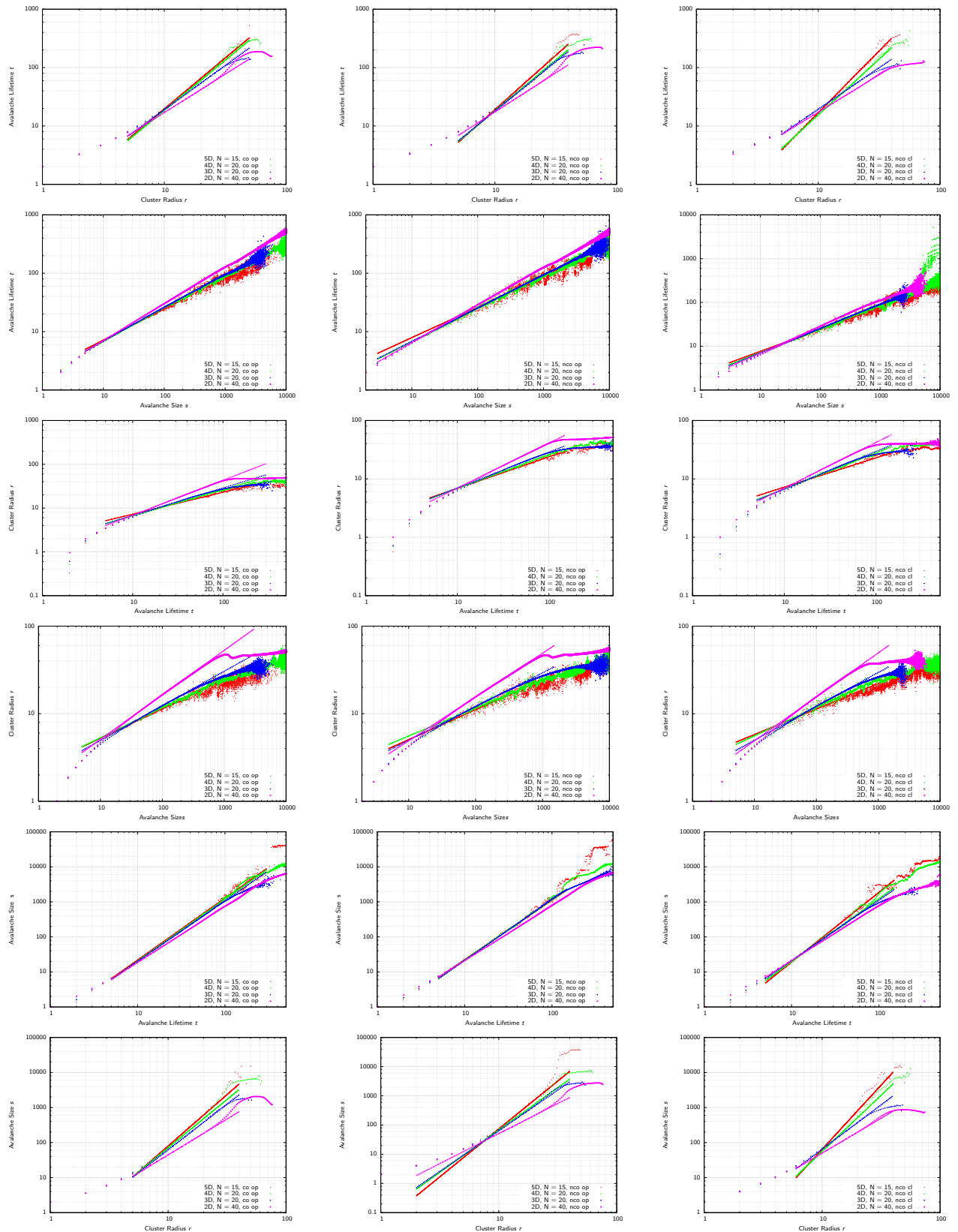


Figure 8. Conditional expectation value distributions for all possible combinations of the three avalanche observables, gained by simulation. Dots give data, dashed lines fitted power law functions

| | | γ_1 | $1/\gamma_1^{-1}$ | γ_2 | $1/\gamma_2^{-1}$ | $\gamma_1\gamma_3$ | γ_3 | $1/\gamma_3^{-1}$ | α | $2 + \frac{\lambda-2}{\gamma_3}$ | τ | $2 + \frac{\lambda-2}{\gamma_2}$ |
|--------|-------|------------|-------------------|------------|-------------------|--------------------|------------|-------------------|----------|----------------------------------|--------|----------------------------------|
| co op | 2D 40 | 1.60 | 1.58 | 2.05 | 2.00 | 2.09 | 1.31 | 1.26 | 2.17 | 2.04 | 2.15 | 2.02 |
| | 3D 20 | 1.72 | 1.75 | 2.60 | 2.56 | 2.59 | 1.51 | 1.61 | 2.66 | 2.47 | 2.40 | 2.27 |
| | 4D 20 | 1.8 | 1.8 | 2.8 | 2.9 | 3.0 | 1.7 | 1.7 | 2.7 | 2.5 | 2.5 | 2.3 |
| | 5D 15 | 1.8 | 1.9 | 2.9 | 3.0 | 3.1 | 1.7 | 2.0 | 3.0 | 2. | 2.6 | 2.3 |
| nco op | 2D 40 | 1.56 | 1.56 | 2.05 | 2.04 | 2.07 | 1.33 | 1.29 | 2.05 | 1.97 | 2.05 | 1.99 |
| | 3D 20 | 1.74 | 1.78 | 2.78 | 2.63 | 2.94 | 1.69 | 1.63 | 2.49 | 2.30 | 2.31 | 2.18 |
| | 4D 20 | 1.7 | 1.8 | 2.9 | 3.2 | 3.0 | 1.7 | 1.7 | 2.7 | 2.9 | 2.3 | 2.6 |
| | 5D 15 | 1.7 | 2.0 | 3.3 | 2.9 | 3.1 | 1.9 | 1.9 | 2.9 | 2.9 | 2.5 | 2.5 |
| nco cl | 2D 40 | 1.58 | 1.63 | 1.98 | 2.00 | 2.02 | 1.28 | 1.28 | 2.07 | 2.02 | 2.03 | 2.01 |
| | 3D 20 | 1.72 | 1.81 | 2.52 | 2.63 | 2.44 | 1.42 | 1.56 | 2.72 | 2.88 | 2.36 | 2.50 |
| | 4D 20 | 1.8 | 1.9 | 3.2 | 3.1 | 3.4 | 1.9 | 1.6 | 2.8 | 2.8 | 2.6 | 2.5 |
| | 5D 15 | 2.0 | 2.0 | 3.7 | 3.4 | 4.2 | 2.1 | 2.0 | 3.2 | 2.8 | 2.6 | 2.5 |

Table 2. Comparison of theoretically equal terms

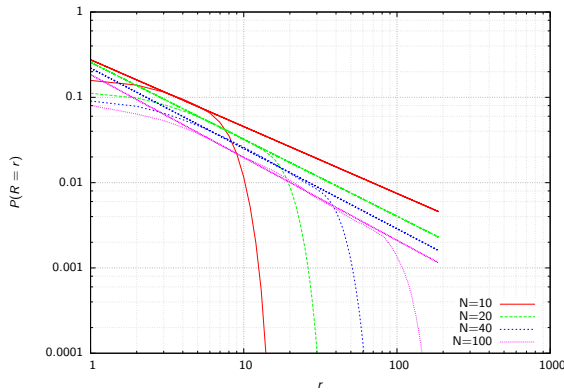
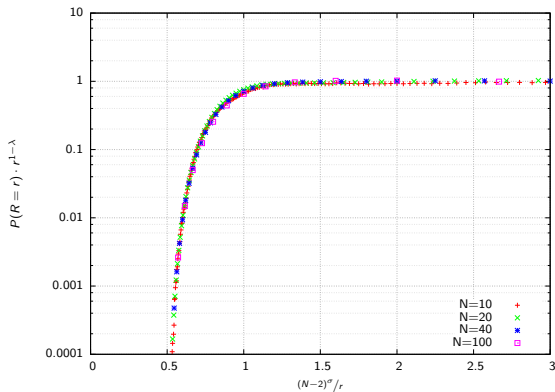

 (a) Probability distributions of R for different lattice sizes N

 (b) Finite size scaling analysis for $\sigma = 1.00$

Figure 9. Finite size scaling analysis

and closed boundaries is (going from one corner to the other and neglecting boundary fields) $2 \cdot (N - 2)$, a linear relation with an exponent $\sigma = 1$.

4 Power Law Behaviour

4.1 $1/f$ -noise in physics

$1/f$ -noise is to be found in many areas in modern physics. One example that may come to mind is electronics, for all electronic devices are subject to $1/f$ -noise. Once a driving current is present, so-called “excess noise” can be observed, which shows a $1/f$ -behaviour. It is also very likely that without the presence of a driving current, resistance fluctuations occur (according to [Wei88]).

Another example are semiconductors. It is very likely that the origin of the noise observed in these devices is a form of charge trapping–detrapping and as such caused by the establishment of a two–state system. A direct measurement is possible by varying the interface density of states, which indeed is proportional to the magnitude of $1/f$ -noise.

$1/f$ -noise can even be the dominant noise up to 1 MHz in SQUID’s (Superconducting quantum interference devices), and the high amount of noise is not fully understood as of [Wei88].

It is also observed that in general, the spectral density scales inversely with the system size, as one would assume when thinking about local independent sources of noise (which can not generally be assumed for all systems discussed here). We will also use this assumption in our analysis of the power spectrum of sandpiles. The observed spectra in real-physics examples scale

in a range of $0.8 < \chi < 1.4$ for the exponent of $f^{-\chi}$ (see [Wei88]), and a low-frequency cutoff is always observed. This is caused by finite size effects or by a breakdown of the system (changing of order or phase of the system, e.g. by crystallisation).

Everyday examples include the noise generated by waterfalls. This noise source can be easily understood using the simple assumption of different sizes of drops of water: Smaller drops can not develop high speeds (because of friction), so they produce noise with lower amplitude hitting the water below (and with higher frequency because of their size). $1/f$ -noise (and as such, also the sound of a waterfall) is also understood as the kind of noise which sounds equally loud in all audible frequency areas to an average human being. Several names for $1/f^\chi$ noise are in use, for $\chi = 1$, “pink noise” is widely used, while “red noise” corresponds to $\chi = 2$. However, these definitions are not always kept and might describe completely different exponents (or be generalised for a wide range of χ).

Concluding the short overview of the occurrence of $1/f$ -noise in physics, no single mechanism can be found to explain all the observed spectra, although the behaviour shows many similarities. As such, an analysis of the sandpile-model may provide further insight into the overall behaviour of a critical system and the dynamics of granular materials (which is important for applications in industry), but not into the general origin of the observed noise. However, a research on the origins of $1/f$ -noise is very useful, as these effects can also be used for measurement themselves: If the origin of the noise is caused by local independent sources, a measurement of the noise allows for the determination of inhomogeneous current patterns, for the expectation is a uniform distribution in a perfect system. Such measurements can be used to find inequalities and disruptions in materials. In this thesis, we will focus on the power spectrum of the sandpile-model and use the assumption that all avalanches are independent, which is a valid approach for such an idealised system.

4.2 Expectation

We can predict the spectrum approximating the f_α with a box function. Utilising the height s/t and the avalanche lifetime t we define (according

to [JCF89]):

$$f_{s,t}(\tau) = s/t \cdot \mathbf{1}_{0 < \tau < T}$$

So $s = \int_0^t s/t d\tau$ is fulfilled trivially. We used the definitions of s and t as provided in section 3. Using a *joint probability distribution* $P(S = s, T = t)$, we can then find the power spectrum as:

$$S(\omega) = \frac{4 \cdot \nu}{(\omega)^2} \int_0^\infty G(\tau) \sin^2\left(\frac{\omega\tau}{2}\right) d\tau$$

$$G(T) = \frac{1}{T^2} \int_0^\infty P(S = s, T = t) \cdot s^2 ds$$

with ν being the total rate of the signals. The complete derivation of this formula has been provided in [JCF89] and shall not be repeated here in detail. The function $G(T)$ is of most interest here, for it allows a prediction of the expected behaviour: Assuming an exponential form of the probability distribution leads to $G(T) \propto T^\alpha \cdot \exp(-T/T_0)$ and the interval which was also selected above should behave as:

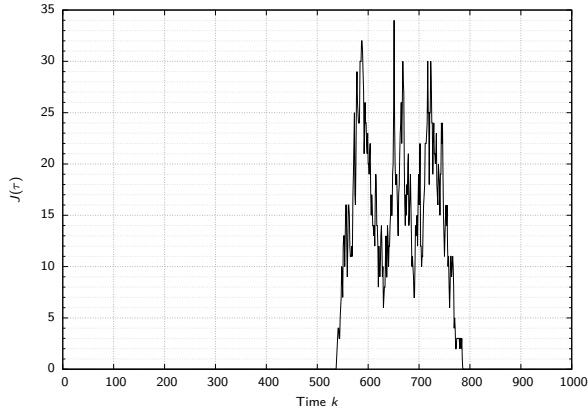
$$S(\omega) = \begin{cases} \omega^{-(3+\alpha)} & \text{if } \alpha < -1 \\ \omega^{-2} & \text{if } \alpha > -1 \end{cases}$$

which corresponds to a $1/\omega^2$ expectation and shows how finite size effects break this expectation for $\alpha < -1$. For lower frequencies $\omega < 1/T_0$, $S(\omega)$ becomes constant (as can also be seen in fig. 11), while for higher frequencies, a falloff with $1/\omega^2$ can be observed. This theoretical observation contradicts the original claims by [BTW87].

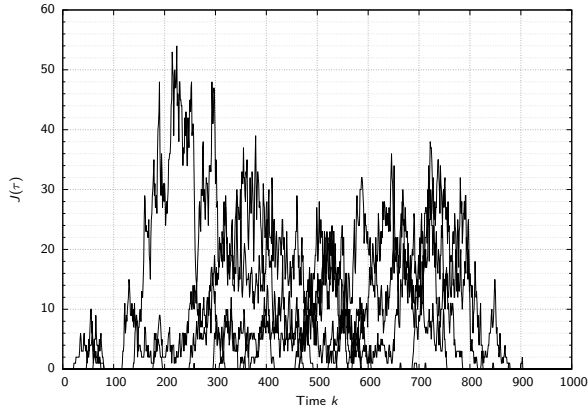
In the following paragraphs, we will analyse whether the physically wide-spread $1/f$ -noise can be found in our system or whether the expected $1/f^2$ -noise is present in the simulated data.

4.3 Process of Measurement

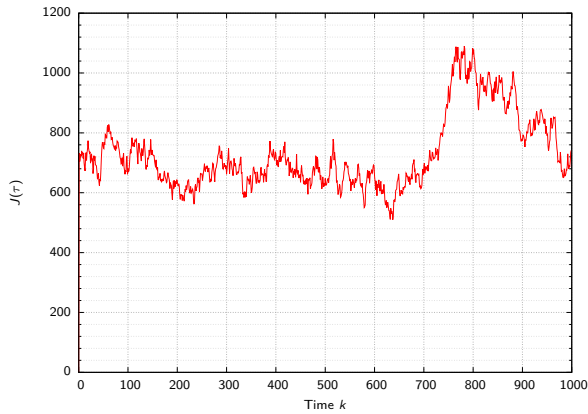
Utilising a high amount of statistics, we can analyse the frequency spectrum directly from our simulated system. To do so, we need to make sure that there is no interference between different avalanches, so we can regard them as individual events, which can be assumed for a sufficiently large system. Algorithmically, the data is taken as described in section 3.2.



(a) The dissipation function of a single perturbation depicted in an arbitrary timescale.



(b) 30 different and independent dissipation functions drawn at random positions into an arbitrary timescale.



(c) The summation of 1000 independent dissipation functions entered at random positions into a fixed time scale.

Figure 10. Analysing the frequency of the system: Building the spectrum from single independent perturbations.

For each avalanche, we introduce an indicator function $p^\alpha(\tau)$ which indicates whether an avalanche α has been triggered in the time range

$\tau, \tau + d\tau$. Dividing the time axis into intervals of length δ , we can then define a *total dissipation rate*, which is the linear overlap of the dissipation rates of the independent perturbation processes (according to [CFJJ91]):

$$j(\tau) := \sum_{\alpha} \sum_{m=-\infty}^{\tau/\delta} f_{\alpha}(\tau - m\delta) p^{\alpha}(m\delta)$$

This new observable is the central measurement variable in the following analyses.

If we now apply many randomly performed perturbations with fixed probability, $p^\alpha(m\delta)$ transforms into a stochastic process $P^\alpha(m\delta)$ (for fixed α), which thus also changes $j(\tau)$ to a stochastic process $J(\tau)$. Algorithmically, this corresponds to adding the dissipations of the single events at a random time position into a dissipation-array of fixed size, whose end is linked to the start of the array thus forming a *ring*. At first, only a single dissipation is added as can be seen in fig. 10a. As more and more dissipations are added, they start to overlap, as shown in fig. 10b.

A summation of the single dissipation functions leads to a simulation of the total dissipation as depicted in fig. 10c. This image already allows for a qualitative analysis of the noise: The superimposed dissipation functions spread over all time scales (as constructed) and the result is more regular than white noise, but less regular than a random walk. These are features of $1/f$ -noise as stated in [BTW88]. Further analysis is done by conducting a Fourier transform.

We use the following discrete transformation rules:

$$\begin{aligned} \Re(f(k)) &= \frac{1}{\sqrt{T}} \cdot \sum_{\tau=0}^T \cos\left(2 \cdot \pi \cdot k \cdot \frac{\tau}{T}\right) \\ \Im(f(k)) &= \frac{1}{\sqrt{T}} \sum_{\tau=0}^T \sin\left(2 \cdot \pi \cdot k \cdot \frac{\tau}{T}\right) \\ |f(k)|^2 &= (\Re(f))^2 + (\Im(f))^2 \end{aligned}$$

And then define the power spectrum:

$$S(f) = \langle |f(k)|^2 \rangle$$

because the obtained spectrum $|f(k)|^2$ is still not very stable. Using many runs, we can use the average $\langle |f(k)|^2 \rangle$ and create a double-logarithmic

| | | co op | nco op | nco cl |
|----|-----|-------|--------|--------|
| 1D | 100 | -1.94 | -3.86 | -3.87 |
| 2D | 20 | -1.42 | – | – |
| 2D | 40 | -1.65 | -1.60 | -1.78 |
| 2D | 100 | -1.63 | -1.60 | -1.61 |
| 3D | 20 | -1.74 | -1.77 | -1.81 |
| 4D | 20 | -1.78 | -1.78 | -1.92 |
| 5D | 15 | -1.79 | -1.88 | -1.80 |
| 6D | 15 | -1.65 | – | – |

Table 3. Exponents of the power law behaviour

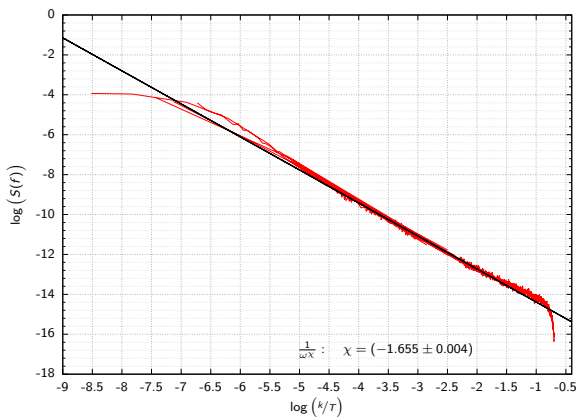


Figure 11. A frequency spectrum for a nonconservative closed system obtained with a dataset of ≈ 15 million perturbations.

plot of $S(f)$ against k/T to visualise a stable frequency spectrum as shown in fig. 11.

This graph basically shows three regions of interest: For lower frequencies, a constant value is observed, then, the power spectrum drops with an $1/f^\chi$ -behaviour, and finally, a fast cutoff can be seen. The near-constant value corresponds to white noise and is caused by finite-size effects, the fast falloff for high frequencies can also be explained with the finite size of the lattice sites themselves.

4.4 Results

As discussed in section 4.3, we performed an analysis of the frequencies for different lattice sizes and dimensions using white-noise perturbation (as also done in section 3.2). The results can be seen in fig. 13 and 12. The frequency behaviour discussed in section 4.2 can be observed for any dimension and lattice size apart

from the 1-dimensional system, in which special cases evolve. This case will only be shown in our results to allow for an easier understanding of the analysis itself, for the 1-dimensional system only shows global avalanches and as such does not behave like a system of self-organised criticality we want to analyse.

A first analysis of the lattice-size dependency is shown in fig. 12. Apparently, although we took high statistics (about 100 million avalanches), the data for small lattices is very noisy. This can be explained with the fact that the initial assumption does not hold anymore: In small lattices, the avalanches can not be regarded as independent, and a continuous perturbation as done in section 4.4 would be necessary. For that reason, we tried to analyse the biggest lattices in every dimension we could still simulate with the computer systems at hand. The data for the 2 dimensional lattice with $N = 100$ seems to be nearly perfect although the taken statistics (50 million perturbations) was smaller.

Analysing the system in different dimensions and with different perturbations, the frequency behaviour is qualitatively similar for all perturbations and dimensions. The 1-dimensional system shows a $1/f^2$ behaviour for conservative perturbation and open boundaries, while for non-conservative perturbation, $1/f^4$ behaviour can be seen. This corresponds to the effects observed in section 2.2: Nonconservative perturbation of a critical state always leads to an avalanche running over the whole system, while conservative perturbation only affects parts of it.

Fitting the exponents using the free tool GNU-PLLOT (see also section 3.2), we can determine whether the qualitative observation is also correct mathematically. We also estimate an error of 0.1 on each exponent, mainly caused by the manual selection of the fitting region. Our results are listed in tab. 3 and in general correspond to the $1/f^2$ behaviour for all systems and perturbation mechanisms.

As can be seen the measured exponents are not exactly -2 as expected for $1/f^2$ behaviour. This deviation is a result of boundary and finite size effects and is compensated by using the function $G(T)$, as explained in section 4.2.

Like already mentioned, another approach using continuous perturbation of the system would allow for the analysis of smaller lattice sizes

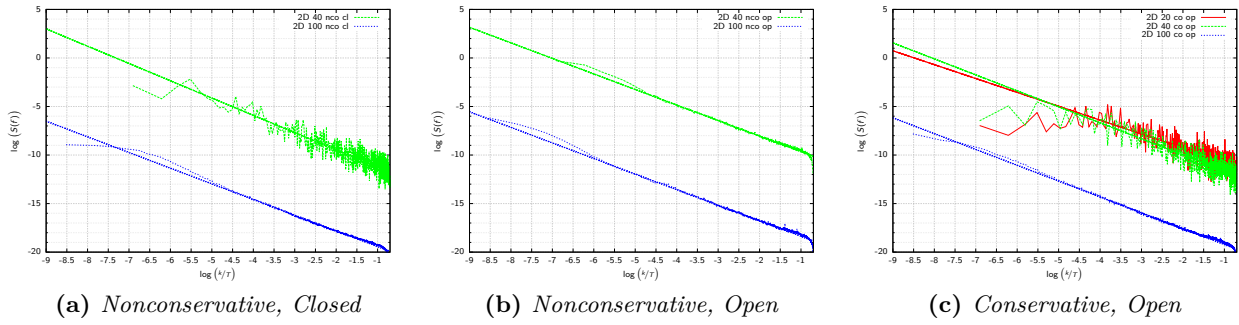


Figure 12. Analysis of frequency spectra for different lattice sizes

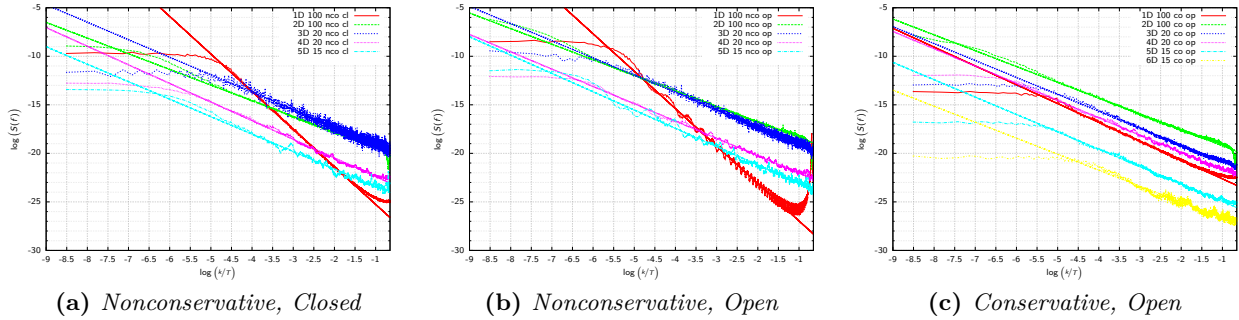


Figure 13. Analysis of frequency spectra for different dimensions

and might provide better statistics. Furthermore, to be able to compare the resulting data with measurements on physical systems, a separate analysis of the dissipation in the interior and on the rim might be of interest, as suggested by [JCF89] and measured experimentally in [JLN89]. This analysis will be performed in the following section.

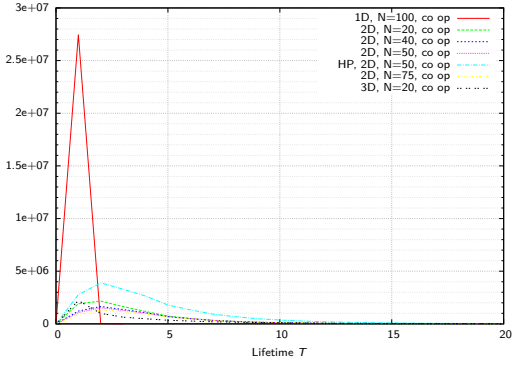
Flow over the Rim One can also analyse the flow over the rim in an open system analogously to a real sandpile as suggested by [JCF89]. This should produce results which can be compared to measured data in experimental setups, and has significant advantages because a different process of measurement is used. Several crucial points are changed: The system is now perturbed randomly at a *constant random* rate, which means a probability that perturbation takes place is used for each step. Concerning the measurement, we continuously save the lengths of pulses on the open rim (i.e. the relaxation of sites on the boundaries in steps of time) and also the time between such pulses. Furthermore, the same observables are measured inside the system. This different perturbation mechanism

allows us to study smaller lattices and to achieve a much higher rate on the rim (and thus lowers the amount of needed calculation steps).

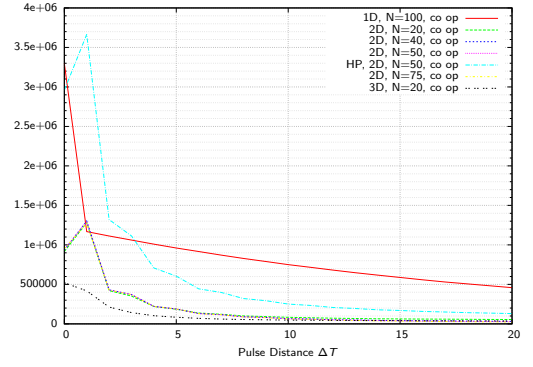
Now, we also want to compare the behaviour with experimental results. As such, we summarise all measured time distances for the specific lifetime of the pulses and create diagrams for the flow over the rim and down the slope.

Analysing fig. 14, one can see that the lifetime-distributions on the rim and in the interior all behave Lorentzian. Differences can be found especially for the 1-dimensional system with conservative perturbation, where the lifetime is nearly constant and the pulse distance is widely spread. The effect of the behaviour in a 1-dimensional system on the frequencies will be discussed later.

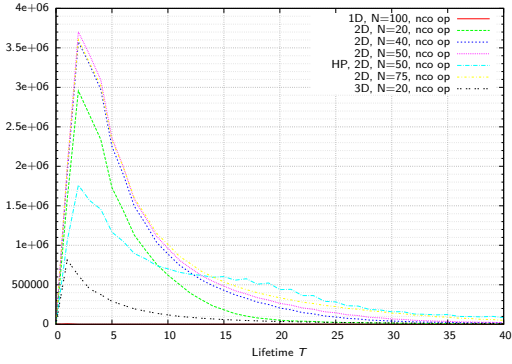
The pulse distances in general appear to fall off exponentially in all dimensions (the 1-dimensional system again behaves differently), while a long tail of the distributions is always present. We can now perform a frequency analysis as already done in section 4.3. As already stated, we will differentiate between dissipation on the open borders and inside the system. Furthermore, the constant perturbation allows us



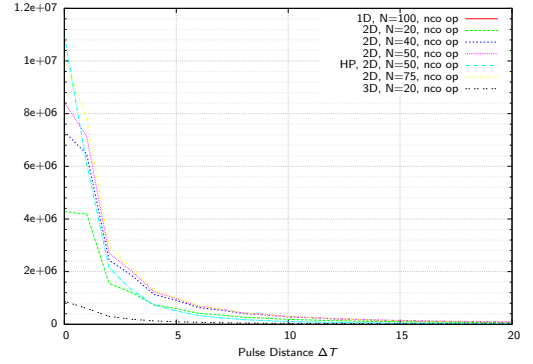
(a) Lifetimes on the rim, conservative



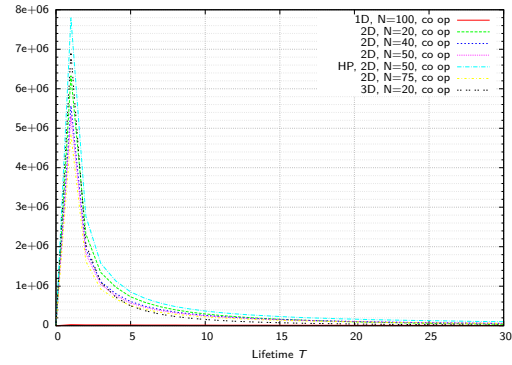
(b) Pulse distance on the rim, conservative



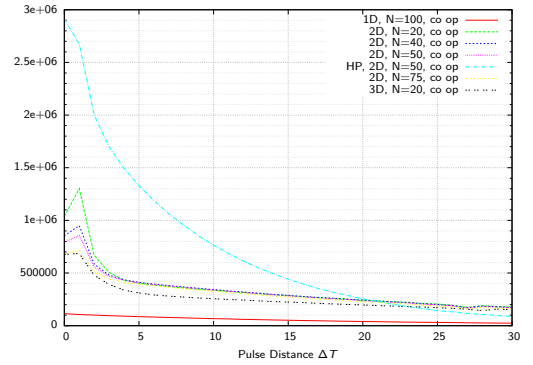
(c) Lifetimes on the rim, nonconservative



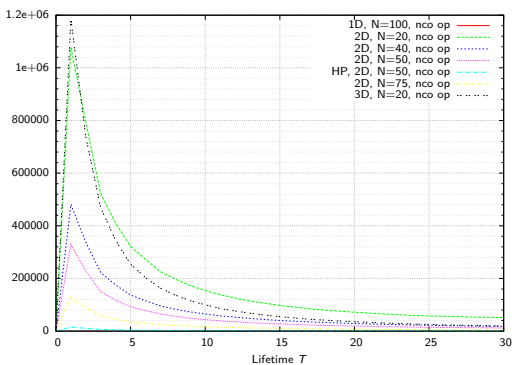
(d) Pulse distance on the rim, nonconservative



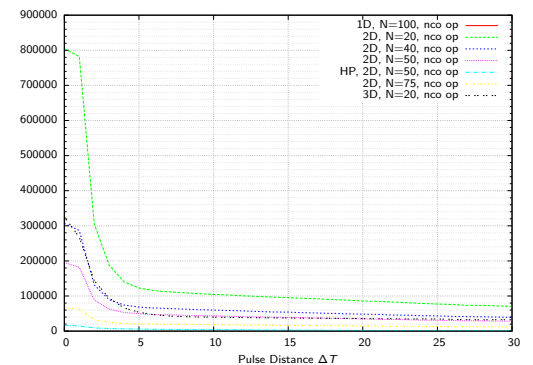
(e) Lifetimes in the interior, conservative



(f) Pulse distance in the interior, conservative



(g) Lifetimes in the interior, conservative



(h) Pulse distance in the interior, conservative

Figure 14. Comparison of Lifetimes and pulse distances in the interior and on the rim in both perturbation mechanisms

| | | Interior | | Rim | |
|----|-----|----------|--------|-------|--------|
| | | co op | nco op | co op | nco op |
| 1D | 100 | -1.82 | -2.36 | -0.07 | 0.00 |
| 2D | 20 | -1.50 | -1.49 | -0.90 | -1.88 |
| 2D | 40 | -1.54 | -1.50 | -0.92 | -1.89 |
| 2D | 50 | -1.54 | -1.50 | -0.92 | -1.89 |
| 2D | 75 | -1.54 | -1.50 | -0.93 | -1.89 |
| 3D | 20 | -1.58 | -1.68 | -1.28 | -1.72 |

Table 4. Exponents of the power law behaviour on the rim and interior

to save all dissipation functions in an array continuously, so no further randomisation (as done previously by inserting the dissipation functions at random points in time) is needed. This is the case because the linear overlap is already performed by the continuous perturbation.

At first, we want to analyse the effect of the used method of perturbation. The boundaries are always open (which in our case means the upper boundaries are open and the lower boundaries are closed), because otherwise there would be no flow of slope on the rim (closed border means $s = 0$). As can be clearly observed in fig. 15, the two methods of perturbation give rise to very different behaviour, which will be analysed in the following paragraphs.

We can find *regular spaced peaks* in the frequencies gained by applying *nonconservative perturbation*. For these data-sets, a probability of 5% was used that another random point is perturbed at each step of time. A higher ratio of perturbation might be of interest to research the origins of the regular patterns. For that reason, we also measured a similar data-set with nonconservative perturbation and a probability of 15% marked by “HP” in the given plots. Analysing the results for nonconservative perturbation, it appears that the resulting data for measurements of flow over the rim can not be used. This can now be explained, because the nonconservative effects lead to an increase in the lifetime of avalanches so the frequency spectrum shows a dependency on the amount of perturbation that is applied. This can be observed in fig. 15. The regularly spaced peaks also appear to depend on the amount of perturbation, and we assume that they are caused by interference

effects between the avalanches on the border. In retrospect, we could not expect physically relevant results for the flow over the rim using nonconservative perturbation, as becomes clear when thinking about the definition: Nonconservative perturbation increases the slope by 1, but changes the heights of the piles on the lattice in a non-physical way as described in section 2.1.

Analysing the results of *conservatively perturbed systems*, we see that there is no influence of the amount of perturbation performed on the spectrum itself. The region of interest for the determination of the exponents appears to be perfectly straight. This is also an important discovery for all measurements performed on the complete power spectra in section 4.4, where the mechanism (single perturbations and overlap of dissipation functions of independent avalanches) is used. This process gives usable results for nonconservative perturbation (because of the independence of the avalanches), but has another flaw for small lattices, as will be discussed later.

We can now take a look at fig. 16 to check the effects of continuous nonconservative perturbation for different dimensions and lattice sizes. As can be seen, the spectra are all influenced by interference of the perturbation, and only a small subset of the high frequencies appears to be “clean” enough to perform a fit. This becomes most apparent in the 1-dimensional system: The continuous perturbation drives the system to high positive slopes close to the open border, which is also the reason why no entries can be seen for the 1-dimensional system in fig. 14c and fig. 14d. The shown data-set includes 5 runs starting with an overcriticalised system and a single run starting with a system resulting from another run. For that reason, two double peaks can be made out marking the size of the positive slope region. The frequencies on the border result in a straight line, as predicted by [JCF89] and becoming apparent when keeping in mind that the open border of a 1-dimensional system is only a single lattice site.

The results for conservative perturbation shown in fig. 17 are of much higher interest for the analysis. The interior frequencies all show very similar behaviour, with the 1-dimensional system showing a different exponent. The frequencies for the flow over the rim also appear to be alike, with the exceptions

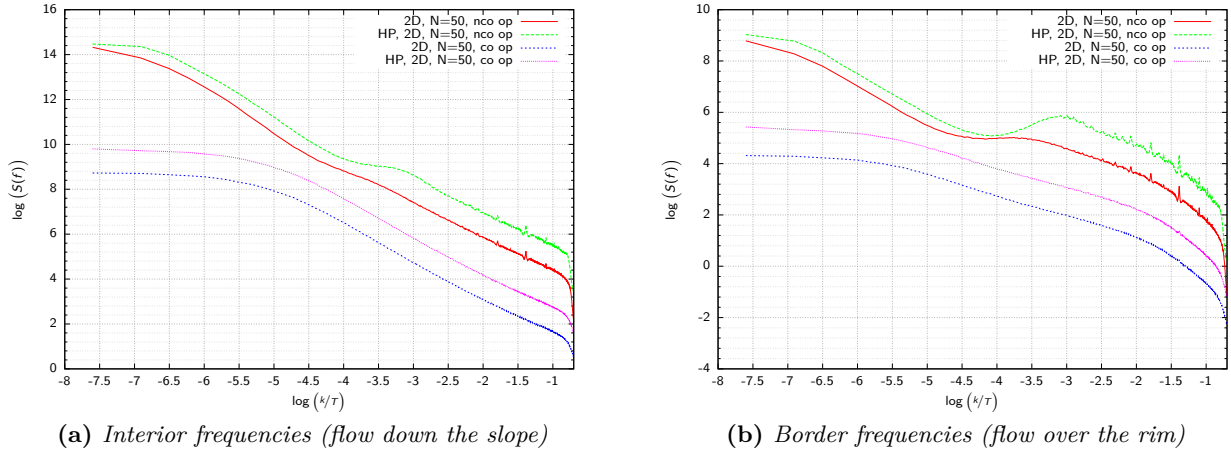


Figure 15. Analysis of the flow over the rim for different methods of perturbation

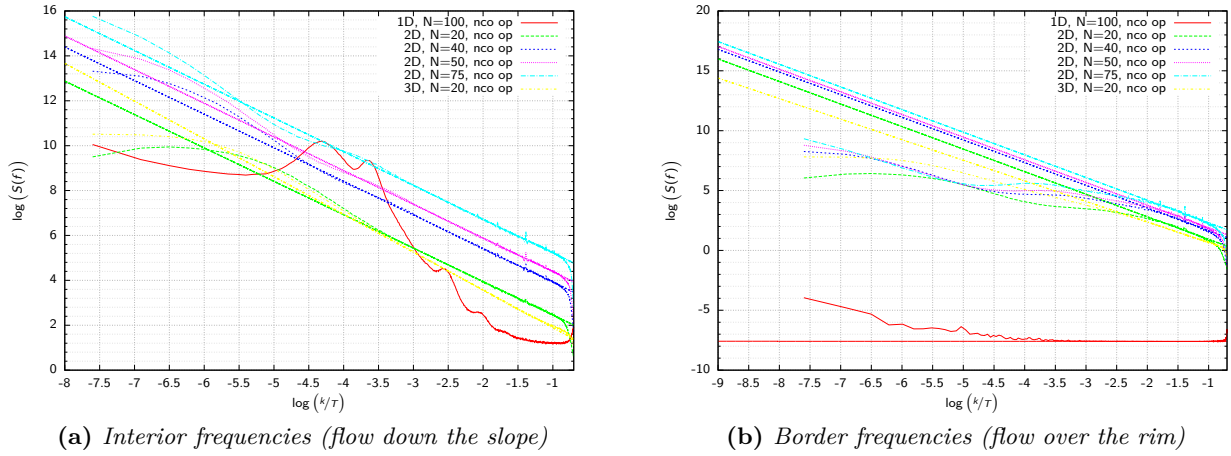


Figure 16. Analysis of the flow frequencies using nonconservative perturbation

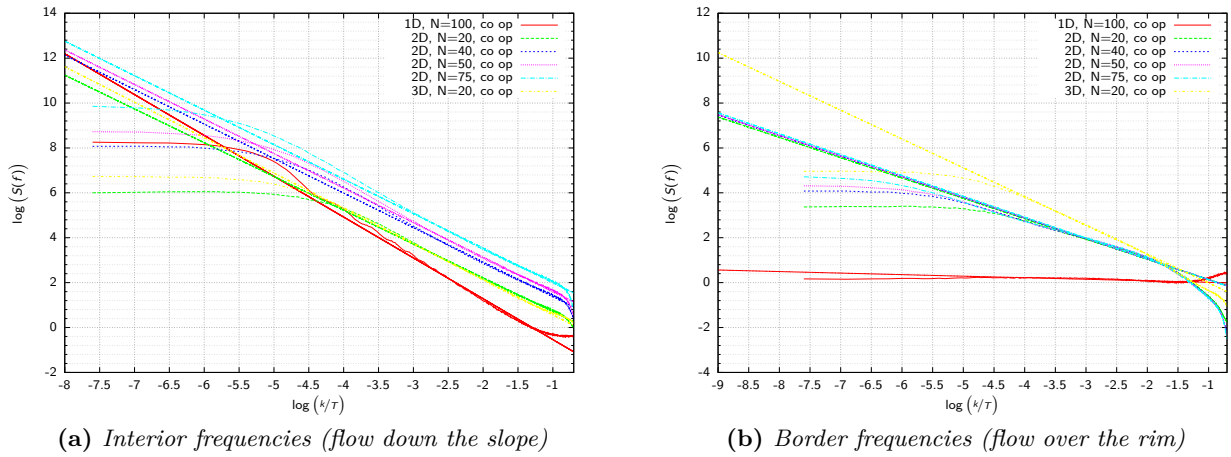
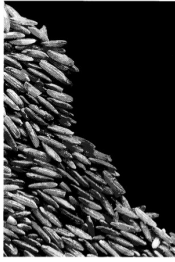


Figure 17. Analysis of the flow frequencies using conservative perturbation



(a) CCD image of rice pile

| TABLE 1 Types of rice used in experiments | | | |
|---|------------------------------------|------------------------------------|------------------------------------|
| | Rice A | Rice B | Rice C |
| Name | Geisha* <i>naturis</i> | Geisha* <i>grtris</i> | Geisha* <i>midtdags/s</i> |
| Description | Unpolished (rough) | Polished (smooth) | Polished (smooth) |
| Length, δ | 7.6 ± 0.9 mm | 4.8 ± 0.4 mm | 6.9 ± 1.0 mm |
| Width | 2.0 ± 0.1 mm | 2.4 ± 0.2 mm | 1.9 ± 0.1 mm |
| Aspect ratio | 3.8 | 2 | 3.6 |
| Average mass, m | 0.02066 g | 0.01840 g | 0.01874 g |
| No. density | 37 ± 1 grains cm^{-3} | 43 ± 1 grains cm^{-3} | 44 ± 1 grains cm^{-3} |
| Energy unit, ϵ | $1.54 \mu\text{J}$ | $0.867 \mu\text{J}$ | $1.27 \mu\text{J}$ |
| Angle of repose | $48.4^\circ \pm 1.2^\circ$ | $46.6^\circ \pm 0.8^\circ$ | $51.1^\circ \pm 0.0^\circ$ |

The large variation in length for rice A and C adds to the inhomogeneity of the system (Fig. 1). The average grain mass, m , was obtained by weighing 2,500 grains. The number density is the average number of grains per unit volume. The energy unit is $\epsilon = mg\delta$, where g is the acceleration of gravity and δ is the grain length. Throughout the Letter we express the energy dissipation in units of ϵ , that is, by the dimensionless quantity $E = \delta/\epsilon$, where δ is the energy dissipation of an avalanche. Similarly, we express the system size L^d by the dimensionless number $L = L^d/\delta$. The average pile height at the vertical wall was used to estimate the angle of repose. The standard deviation in this angle reflects the observed height fluctuations.

* Geisha is a registered trademark from Staburet a.s. (Trollåsen, Norway).

(b) Data table of different rice types

Figure 18. Experiment to analyse the frequency spectrum of piles built by different types of rice ([FCMS⁺96])

being the 1–dimensional system with an exponent close to zero (as expected) and a slightly larger exponent than for all other dimensions in the 3–dimensional system. We use the free tool GNUPLOT (see also section 3.2) to fit the exponents, assuming an error of 0.1 on each exponent caused by the manual selection of the fitting region. The nonconservative exponents are only given for reasons of comparison, but they should be interpreted with great caution, because we assume errors in the order of 0.5 caused by the interferences of the perturbation. The results for the exponents are given in tab. 4 and the orders of magnitude and qualitative behaviour also correspond to the observation in experiments performed with sand, which have for example been performed in [JLN89].

5 Conclusion and Outreach

5.1 Outreach

We have shown only a little part of possible considerations dealing with the BTW model of sandpiles. Interesting extensions are for example a continuation of the rules, which then leads to the BURRIDGE–KNOPOFF–model, which can be used to describe the evolution of earthquakes (see [CO92]). Also the fact that the critical slope can depend on the actual form of the grains can be taken into account by using dynamical varying critical slopes (see [Fre93]).

As already mentioned at certain points, there have also been performed some real experiments in order to test the predictability of the model, like [FCMS⁺96] or [JLN89], where the focus lied on the power spectra. They come to the result,

that at some specific aspects, $1/f$ and $1/f^2$ can be seen, but also that there is much more than the theory considers, like hysteresis in the critical slope value or different tumbling mechanisms taking into account the actual size and form of the individual grains. This was interesting, since BAK–TANG and WIESENFELD] assumed ([BTW87]) that at the critical state of such a self–organized system, internal structures do not play a role anymore and that only the global behaviour of the system is important, which clearly was falsified using different internal structures (like different types of rice, see fig. 18) and showing that the critical system behaves differently then.

5.2 Summary

We have introduced the BAK–TANG–WIESENFELD–model of sandpiles and how it drives itself into an attractive state by the principle of self–organized criticality. Analysing the properties of avalanches occurring when perturbing the critical pile has shown us why the attractor is indeed critical and that these properties fulfill power law behaviours, whose critical exponents we determined by simulating the model and fitting to our numerical data. We have seen that theoretically derived scaling relations could be verified within numerical accuracy. Analysing the power spectra, we confirmed a general $1/f^2$ behaviour for spectra of the whole lattice across all checked dimensions (up to 6D) and could also compare our data with experimental observations when performing separate analyses for the interior and the flow over the open rim.

References

- [BTW87] Bak, Per, Chao Tang, and Kurt Wiesenfeld: *Self-organized criticality: An explanation of the $1/f$ noise*. Phys. Rev. Lett., 59(4):381–384, Jul 1987.
- [BTW88] Bak, Per, Chao Tang, and Kurt Wiesenfeld: *Self-organized criticality*. Phys. Rev. A, 38(1):364–374, Jul 1988.
- [CFJJ91] Christensen, Kim, Hans C. Fogedby, and Henrik Jeldtoft Jensen: *Dynamical and spatial aspects of sandpile cellular automata*. Journal of Statistical Physics, 63:653–684, 1991, ISSN 0022-4715. <http://dx.doi.org/10.1007/BF01029204>, 10.1007/BF01029204.
- [CO92] Christensen, Kim and Zeev Olami: *Scaling, phase transitions, and nonuniversality in a self-organized critical cellular-automaton model*. Phys. Rev. A, 46(4):1829–1838, Aug 1992.
- [CO93] Christensen, Kim and Zeev Olami: *Sandpile models with and without an underlying spatial structure*. Phys. Rev. E, 48(5):3361–3372, Nov 1993.
- [FCMS⁺96] Frette, Vidar, Kim Christensen, Anders Malthe-Sorensen, Jens Feder, Torstein Jossang, and Paul Meakin: *Avalanche dynamics in a pile of rice*. Nature, 379(6560):49–52, Jan 1996. <http://dx.doi.org/10.1038/379049a0>.
- [Fre93] Frette, Vidar: *Sandpile models with dynamically varying critical slopes*. Phys. Rev. Lett., 70(18):2762–2765, May 1993.
- [JCF89] Jensen, Henrik Jeldtoft, Kim Christensen, and Hans C. Fogedby: *$1/f$ noise, distribution of lifetimes, and a pile of sand*. Phys. Rev. B, 40(10):7425–7427, Oct 1989.
- [JLN89] Jaeger, H. M., Chu heng Liu, and Sidney R. Nagel: *Relaxation at the angle of repose*. Phys. Rev. Lett., 62(1):40–43, Jan 1989.
- [Wei88] Weissman, M. B.: *$1/f$ noise and other slow, nonexponential kinetics in condensed matter*. Rev. Mod. Phys., 60(2):537–571, Apr 1988.
- [WKm08] Williams, Thomas, Colin Kelley, and many others: *Gnuplot 4.4: an interactive plotting program*. <http://gnuplot.sourceforge.net/>, October 2008.